PROCEEDINGS OF SCIENCE

Measurements of the elastic cross section $d\sigma/dt$ in $p\bar{p}$ scattering at $\sqrt{(s)} = 1.96$TeV

Vladislav Simak, for D0 experiment*

Czech Technical University in Prague, Faculty of Nuclear Sciences and Physical Engineering, Brehova 7, 115 19, Prague 1, Czech Republic, and Institute of Physics, Academy of Sciences of the Czech Republic, Na Slovance 2, 182 21, Prague 8, Czech Republic

E-mail: simak@fzu.cz

We present a measurement of the elastic differential cross section $d\sigma(p\bar{p} \to p\bar{p})/dt$ as a function of the four-momentum-transfer squared t. The data sample corresponds to an integrated luminosity of $\approx 31nb^{-1}$ collected with the D0 detector using dedicated Tevatron $p\bar{p}$ Collider operating conditions at $\sqrt{(s)} = 1.96TeV$ and covers the range $0.26 < |t| < 1.2GeV^2$. For $|t| < 0.6GeV^2$, $d\sigma/dt$ is described by an exponential function of the form $Ae^{-b|t|}$ with a slope parameter $b = 16.86 \pm 0.10(stat) \pm 0.20(syst)GeV^{-2}$. A change in slope is observed at $|t| \approx 0.6GeV^2$, followed by a more gradual $|t|$ dependence with increasing values of $|t|$ [1].

36th International Conference on High Energy Physics
4-11 July 2012
Melbourne, Australia

*Speaker.

PoS(ICHEP2012)284

1. Introduction

We present a measurement of the $p\bar{p}$ elastic differential cross section at $\sqrt{(s)} = 1.96TeV$ in the range $0.26 < |t| < 1.2GeV^2$, measured using the forward proton detector (FPD) spectrometer system of the D0 experiment [2] . Since p and $\bar{p}$ elastic scattering angles are typically very small (on the order of milliradians), they are not covered by the main D0 detector. The elastically scattered protons and antiprotons are tagged with detectors inserted in the beam pipe on either side of the interaction point (IP). Our measurement extends the |t| range previously studied by the CDF ($0.025 < |t| < 0.29GeV^2$) [3] and by the E710 ($0.034 < |t| < 0.65GeV^2$) [4]. Collaborations at the Tevatron and constitutes the first confirmation of a change in the |t| dependence of $d\sigma(p\bar{p} \to p\bar{p})/dt$ at center-of-mass energy $\sqrt{(s)} = 1.96$ TeV. A similar measurement in pp collisions at $\sqrt{(s)} = 7.0$ TeV has recently been reported by the TOTEM Collaboration [5] showing similar trends for the slope of the differential cross section and for the position of the local diffraction minimum, although the local minimum found in pp elastic scattering is much more pronounced than the kink we observe.

2. D0 and Forward Proton Detector

A detailed description of the D0 detector can be found in reference [2]. The central tracking system of the D0 detector comprises a silicon microstrip tracker (SMT) and a central fiber tracker (CFT), surrounded by a 2 T superconducting solenoidal magnet. The pseudorapidity, (defined as $\eta = -ln[tan(\Theta/2)]$, where Θ is the polar angle with respect to the proton beam direction) coverage for the tracking detectors is $|t| < 3$ for the SMT and $|t| < 2.5$ for the CFT. Outside of the superconducting magnet, the liquid-argon and uranium calorimeter is composed of three sections housed in separate cryostats: a central calorimeter section covering the pseudorapidity range $|t| < 1.1$ and two end calorimeter sections that extend coverage to $|t| \approx 4.2$ [6]. The luminosity monitor (LM) consists of plastic scintillator arrays located at $z \pm 140cm$ (where z is measured from the interaction point (IP) along the nominal direction of the proton beam), and covers the pseudorapidity range $2.7 < |t| < 4.4$. The LM is used to detect non-diffractive inelastic collisions and to make an accurate determination of the luminosity.

Forward Proton Detectors Fig.1. shows the layout of the main components of the FPD system relevant to this measurement [2]. In the center of the diagram is the interaction point, IP, at the center of the main D0 detector. A scattered proton/antiproton goes through 3 Tevatron quadrupole magnets which alternate defocusing in the horizontal and vertical planes.

The FPD consists of four quadrupole spectrometers on both the scattered proton (P) and scattered antiproton (A) sides plus a dipole spectrometer. Each quadrupole spectrometer is composed of two scintillating fiber detectors, one located at about 23 m (A1 or P1) and the second at about 31 m (A2 or P2) from the IP along the Tevatron beam line. Both detectors are either above (U), below (D), on the inner side (I), or on the outer side (O) of the beam line. The pseudorapidity range covered by the detectors is about $7.3 < |t| < 8.6$.

Scattered protons and antiprotons cross thin stainless steel windows at the entrance and exit of a vessel (Roman pot) containing the detectors [7]. The pots are remotely controlled and moved to within a few millimeters of the beam during stable beam conditions. The Roman pots house

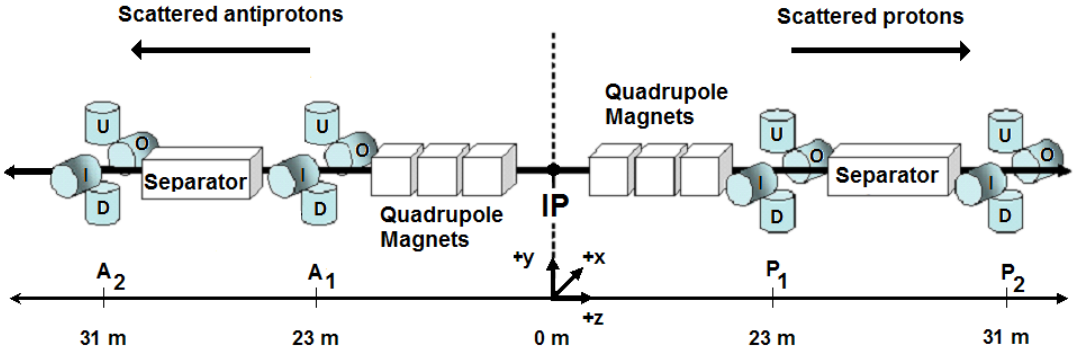

Figure 1: Schematic view of the Roman pot stations (A1, A2, P1, P2). The letters U, D, I, O make reference to the up, down, inner and outer detectors, respectively.

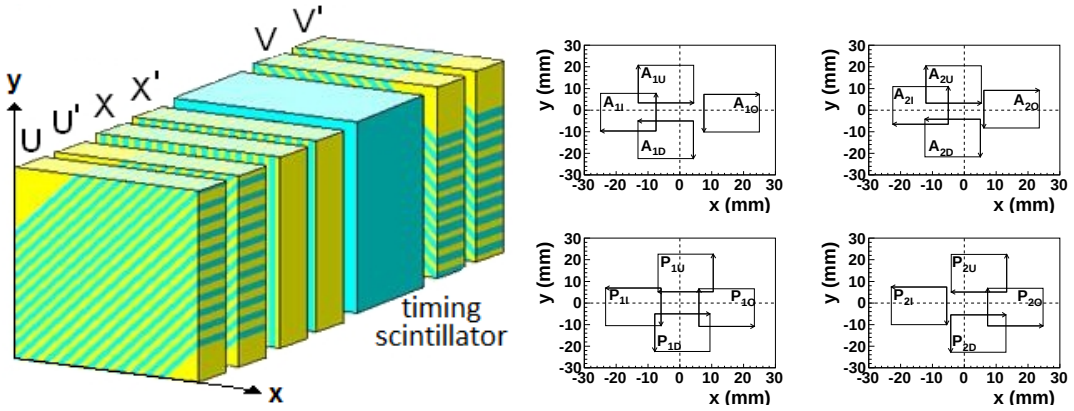

Figure 2: Schematic view of the design of one FPD scintillating fiber detector. The local detector x, y coordinates are indicated by the arrows. The scintillating fibers are indicated by the stripes (left). Detector positions with respect to beam center (dashed lines) for the data set corresponding to the closest pot insertion to the beam (right).

position detectors using 0.8 mm x 0.8 mm square double-clad polystyrene scintillating fibers to detect the passage of charged particles. Each position detector consists of six layers of scintillating fibers , where the scintillating fibers of the layers are rotated by ±45 degrees. Fig. 2.

Each detector also contains a scintillator (read out by a time-to-digital converter system) which provides a time measurement for particles passing through the detector with a resolution of about 1 ns. The time measurement is used to distinguish particles coming from the center of the D0 detector from background beam halo particles (particles traveling far enough outside of the main beam core that they pass through the FPD detector).

Beyond the active areas of the detectors, matching square clear fibers transport signals from the scintillators to 16-channel multi-anode photomultiplier tubes. The electronic signals are subsequently amplified, shaped, and sent to the D0 triggering and data acquisition system [2].

3. Data and reconstruction

An initial data sample is obtained by requiring events to satisfy one of the elastic triggers. The

p and $\bar{p}$ hit coordinates are measured in the FPD system using the fibers information and then used to select the sample of elastic scattering events. We align the detectors with respect to the beam and then use the beam transport matrices (which are functions of the currents of the magnets located between the IP and the FPD detectors and correlate the x, y coordinates and scattering angle of a particle at two specific z locations) to reconstruct the paths of protons and antiprotons through this region of the Tevatron.

The data for this analysis were collected with dedicated beam conditions designed to facilitate the positioning of the FPD Roman pots as close to the beam axis as possible. The Tevatron injection tune with the betatron function of $\beta^* = 1.6m$ at the D0 IP was used instead of the standard $\beta^* = 0.35m$ lattice. Additionally, only one proton bunch and one antiproton bunch were present in the Tevatron.

Approximately 20 million events were recorded using a special trigger list optimized for diffractive physics, including triggers for elastic, single diffractive, and double pomeron exchange. This analysis uses elastic triggers, which make up about 10% of the total data collected.

Events with more than four fibers firing in a plane are typically not due to single particles and are rejected (more than 99% of the elastic triggered events survive this condition). We require at least two out of the three fine segments to be reconstructed in each detector, with their intersection yielding the transverse coordinates of the hit.

4. Elastic Event Selection

Elastic collisions produce one of the four possible hit configurations in the FPD: AUPD, ADPU, AIPO, AOPI. If we compare the hit coordinates reconstructed by each of the two detectors of one spectrometer, we observe a correlation band from particles going through the spectrometer, but also observe some uncorrelated background hits (see Fig. 4 left).

For the data collected with the Roman pots retracted further away from the beam line, we use positional difference information obtained from the pot motion system added to the previously determined aligned positions. The uncertainty of the location of the detectors after the alignment procedure is estimated to be about 200 μ.

The primary source of background in the selected sample is due to beam halo, consisting of either a halo proton and a halo antiproton in the same bunch crossing or a halo particle combined with a single diffractive event. A halo particle passing through the proton detectors in the time window for the protons which have undergone elastic scattering usually passes through the diagonally opposite antiproton detector at an earlier time. Therefore, the time information can be used to veto events with early time hits, consistent with halo protons and antiprotons in the elastic sample.

The absolute uncertainty of the background, which is propagated as a statistical uncertainty to $d\sigma/dt$, varies from 0.3% at low |t| to 5.0% at high |t|. As a cross check, we vary the detector band cuts from 3.0σ to 3.5σ and to 6.0σ, to allow more background, and obtain similar dN/dt results after applying the same background subtraction procedure (within 1%).

5. Monte Carlo Simulation and Results

We have developed a MC generator interfaced with the Tevatron transport matrices to generate elastic events. The MC allows us to study the geometrical acceptance of the detectors, resolution

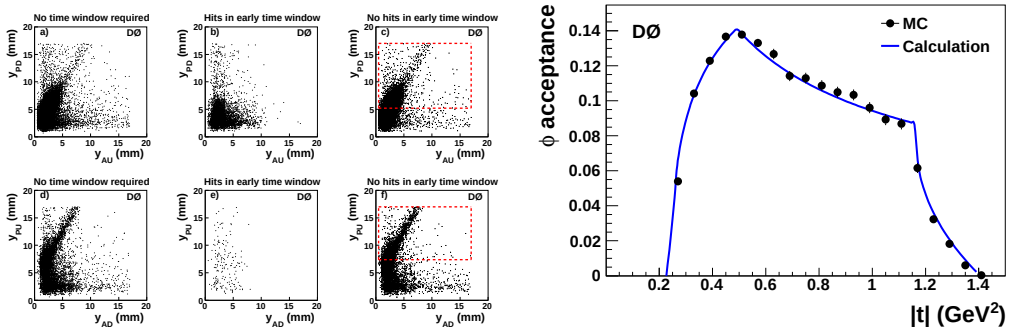

Figure 3: The correlation plots for the first detectors in the spectrometers (y coordinates measured in the local coordinate system shown for AUPD and ADPU. The dashed lines correspond to the fiducial requirements applied (left). Azimuthal acceptance of the FPD in data, after fiducial cuts, for the closest detector position of the AUPD elastic combination. The points correspond to MC, the solid line corresponds to the calculation of the ϕ acceptance from the detector positions and the fiducial area (right).

of the position measurement, alignment, and effects of the beam size and beam divergence at the IP. The generation of events is based on an Ansatz function that we obtain by fitting the dN/dt distribution of the data.

We obtain results for the ϕ acceptance using the MC described in the previous section before adding the effects of beam divergence, IP size and detector resolution. The uncertainty in the ϕ acceptance correction, which comes from the size of the MC sample used, is less than 0.1% at low |t| values and less than 1.0% at high |t| values Fig.4 right.

In total, we have four independent measurements of $d\sigma/dt$ that come from the two elastic combinations (AUPD and ADPU) and two data sets, which agree with each other within the uncertainties. We combine the four measurements using a bin-by-bin weighted average. The resulting values for the $d\sigma/dt$ distribution, together with their total uncertainties, are shown in Fig. 4 left. The uncertainties are the total experimental uncertainties excluding the 14.4% normalization uncertainty. The |t| bin centers are determined using the prescription described in [9], however, the values found are very close to the middle of the bin. Two phenomenological model predictions for $\sqrt{(s)} = 1.96TeV$ ([10] and [11]) are also shown. The BSW model shows a good description of the data in shape and normalization and is able to reproduce the kink within experimental uncertainties.

The |t| range covered by our measurement is $0.26 < |t| < 1.2$ GeV2. We observe a change in the logarithmic slope of the $d\sigma/dt$ distribution at $|t| \approx 0.6GeV^2$. A fit to the $d\sigma/dt$ distribution in the range $0.26 < |t| < 0.6$ with an exponential function of the form $Ae^{-b|t|}$ yields a logarithmic slope parameter of $b = 16.86 \pm 0.10(stat) \pm 0.20(syst)GeV^{-2}$. Fig. 4 right shows a comparison of our results to those obtained at $\sqrt{(s)} = 1.8TeV$ by the CDF and E710 Tevatron Collaborations [11, 12], and also to that of the UA4 Collaboration at $\sqrt{(s)} = 0.546TeV$ [12]. Our measurement of the slope parameter agrees within uncertainties with previous measurements by the CDF (b = 16.98 ± 0.25 GeV^{-2}) and E710 (b = 16.30 ± 0.30 GeV^{-2}) Collaborations.

A comparison of the shape of our measured $d\sigma/dt$ to UA4 measurement shows that the kink in $d\sigma/dt$ moves towards lower |t| values as the energy is increased, but, as in the UA4 data, we do not see a distinct minimum as observed in pp elastic interactions [12].

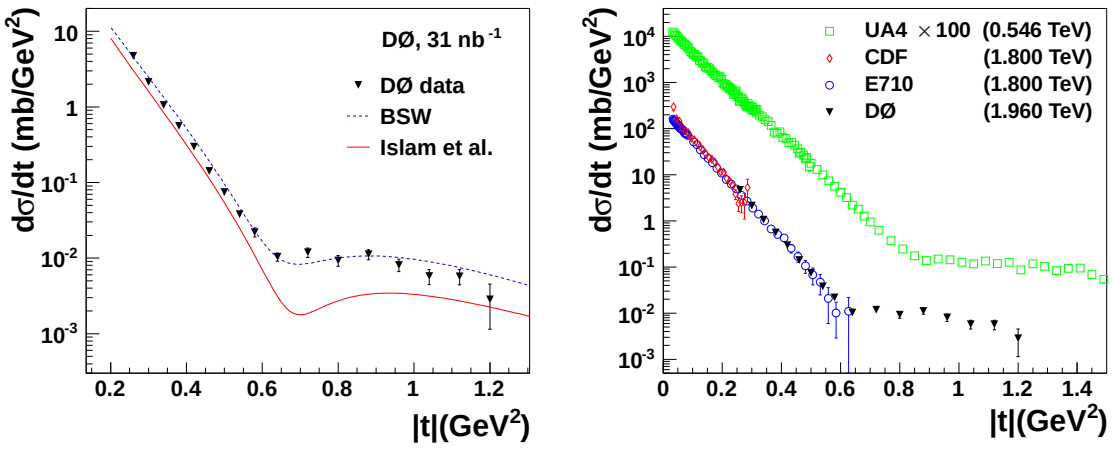

Figure 4: The measured $d\sigma/dt$ differential cross section. The predictions of BSW ([25]) and Islam et al. ([26]) are compared to the data (left). The $d\sigma/dt$ differential cross section measured by the D0 Collaboration and compared to the CDF and E710 measurements at $\sqrt{(s)} = 1.8TeV$, and to the UA4 measurement at $\sqrt{(s)} = 0.546TeV$ (right).

In summary, we have presented the first measurement of $d\sigma(p\bar{p} \to p\bar{p})/dt$ as a function of |t| at $\sqrt{(s)} = 1.96$ TeV. Our measurement extends the |t| and ps range previously studied and shows a change in the |t| dependence, consistent with the features expected for the transition between two diffractive regimes.

References

[1] V. M. Abazov et al. (D0 Collaboration), Phys. Rev. D 86, 012009 (2012).

[2] V. M. Abazov et al. (D0 Collaboration), Nucl. Instr. Meth. Phys. Res. A 565, 463 (2006).

[3] F. Abe et al. (CDF Collaboration), Phys. Rev. D 50, 5518 (1994).

[4] N. Amos et al. (E710 Collaboration), Phys. Lett. B 247, 127 (1990).

[5] G. Antchev et al.(TOTEM Collaboration), Eur. Phys. Lett. 95, 41001 (2011).

[6] S. Abachi et al. (D0 Collaboration), Nucl. Instr. Meth. Phys. Res. A 338, 185 (1994).

[7] U. Amaldi et al., Phys. Lett. B 44, 112 (1973).

[8] V. M. Abazov et al. (D0 Collaboration), Phys. Rev. Lett. 101, 062001 (2008).

[9] G. Laferty and T. Wyatt, Nucl. Instr. Meth. Phys. Res. A 355, 541 (1995).

[10] C. Bourrely, J. Soffer, and T.T. Wu, Eur. J. Phys. C 28, 97 (2003).

[11] M. M. Islam, J. Kaspar, R. J. Luddy, and A. V. Prokudin, in Proceedings of the 13th International Conference on Elastic and Diffractive Scattering, CERN, Geneva, June- July 2006, arXiv:1002.3527 [hep-ph].

[12] M. Bozzo et al. (UA4 Collaboration), Phys. Lett. B 155, 197 (1985).